Received: 24 February 2022 | Revised: 14 September 2022 | Accepted: 21 September 2022

DOI: 10.1096/fj.202200289RR

THE FASEB JOURNAL

RESEARCH ARTICLE

Muscle injury induces a transient senescence-like state that is required for myofiber growth during muscle regeneration

Laura V. Young[1] | **Griffen Wakelin**[1] | **Alasdair W. R. Cameron**[1] | **Stevan A. Springer**[1] | **Joel P. Ross**[1] | **Grant Wolters**[1] | **J. Patrick Murphy**[1] | **Michel G. Arsenault**[1] | **Sean Ng**[2] | **Nicolás Collao**[3] | **Michael De Lisio**[3] | **Vladimir Ljubicic**[2] | **Adam P. W. Johnston**[1,4,5]

[1]Department of Applied Human Sciences, University of Prince Edward Island, Charlottetown, Prince Edward Island, Canada

[2]Department of Kinesiology, McMaster University, Hamilton, Ontario, Canada

[3]School of Human Kinetics, University of Ottawa, Ottawa, Ontario, Canada

[4]Department of Biomedical Sciences, University of Prince Edward Island, Charlottetown, Prince Edward Island, Canada

[5]Dapartment of Medical Neuroscience, Dalhousie University, Halifax, Nova Scotia, Canada

Correspondence
Adam P. W. Johnston, Department of Medical Neuroscience, Dalhousie University, Halifax, Nova Scotia, B3H 4R2, Canada.
Email: adamjohnston@dal.ca

Funding information
Natural Sciences and Engineering Research Council of Canada, Grant/Award Number: RGPIN-2016-05747

Abstract

Cellular senescence is the irreversible arrest of normally dividing cells and is driven by the cell cycle inhibitors *Cdkn2a*, *Cdkn1a*, and *Trp53*. Senescent cells are implicated in chronic diseases and tissue repair through their increased secretion of pro-inflammatory factors known as the senescence-associated secretory phenotype (SASP). Here, we use spatial transcriptomics and single-cell RNA sequencing (scRNAseq) to demonstrate that cells displaying senescent characteristics are "transiently" present within regenerating skeletal muscle and within the muscles of D2-*mdx* mice, a model of Muscular Dystrophy. Following injury, multiple cell types including macrophages and fibrog–adipogenic progenitors (FAPs) upregulate senescent features such as senescence pathway genes, SASP factors, and senescence-associated beta-gal (SA-β-gal) activity. Importantly, when these cells were removed with ABT-263, a senolytic compound, satellite cells are reduced, and muscle fibers were impaired in growth and myonuclear accretion. These results highlight that an "acute" senescent phenotype facilitates regeneration similar to skin and neonatal myocardium.

KEYWORDS
muscle, regeneration, senescence, single-cell RNA sequencing

1 | INTRODUCTION

Senescence is a multifaceted stress response typified by irreversible growth arrest of cells normally capable of cell division.[1] Cellular senescence plays a pivotal role in cellular aging, and age-related chronic conditions such as Alzheimer's,[2] cardiovascular disease,[3] and cancer.[4] Cells enter senescence through various mechanisms including

Abbreviations: APC, antigen-presenting cell; CSA, cross-sectional area; FAPs, fibro-adipogenic progenitors; GO, gene ontology; H&E, hematoxylin and eosin; OCT, optimal cutting temperature compound; PBS-T, tween in PBS; PCA, principal component analysis; SA-β-gal, senescence-associated beta galactosidase; SASP, senescence-associated secretory phenotype; scRNAseq, single-cell RNA sequencing; UMAP, uniform manifold approximation and projection; UMI, unique molecular identifier.

oxidative damage, genomic instability, and widespread tissue injury. These stimuli initiate a senescence response by engaging cell cycle inhibitors such as $p16^{INK4a}$, $p21^{Cip1}$, and p53 which induce permanent growth arrest.[5] Senescent cells frequently remodel the local cellular environment by secreting cytokines, chemokines, proteases, and soluble factors collectively known as the "senescence-associated secretory phenotype" (or SASP)[6] which also serves to recruit immune cells.

Our understanding of cellular senescence extends beyond aging and chronic disease as recent work has uncovered novel functions of senescent cells in tissue regeneration and morphogenesis. Indeed, transitory senescent cell activity is required for skin wound repair[7] and neonatal cardiac regeneration.[8] However, little is known regarding the role of "acute" senescence in other tissues with high regenerative capabilities such as skeletal muscle. Indeed, while satellite cell senescence contributes to age-related muscle loss,[9] a function for cellular senescence in normal muscle repair has not been described.

Spatial transcriptomics represents the evolution of single-cell RNA sequencing (scRNAseq) and provides the spatial location (on a tissue section) of whole transcriptome sequencing. Spatial transcriptomics (such as Visium from 10x Genomics) captures the RNA from a tissue section on a slide using a printed spatial array of dots which consist of uniquely barcoded beads with oligonucleotides to capture polyadenylated RNA for sequencing.[10] Due to the barcoding, the RNA is then mapped back to the dot of origin and aligned with a hemaotoxylin and eosin (H&E) stain of the same section to overlay morphology with gene expression. Spatial transcriptomics technologies are now widely implemented to study tissue and disease biology in diverse fields from neuroscience to cancer.[11]

Here, we use a combination of scRNAseq, spatial transcriptomics, and functional in vivo assays to define a novel mechanism governing muscle repair which relies on the transient appearance of cells displaying senescent features following myotrauma. We reveal that multiple cell types display senescence-like features by upregulating a core signature of senescence-related genes including *Cdkn1a*, *Trp53*, and the regenerative SASP factor *Cyr61* (CCN1). This response is not limited to cardiotoxin (CTX)-induced injury as senescent-like cells are also present within the muscles of D2-*mdx* mice, a model of Muscular Dystrophy. Importantly, the removal of cells with senescent characteristics via the senolytic compound ABT-263 abrogates muscle repair and growth following CTX-induced injury while reducing satellite cell content.

2 | MATERIALS AND METHODS

2.1 | Mice and animal procedures

All animal procedures and ethics were approved by the University of Prince Edward Island Animal Care Committee in accordance with CCAC guidelines (AUP #16-036). Eight-week-old male C57BL/6 mice were purchased from Charles River Laboratories. For muscle regeneration timecourse experiments ($n = 6$ per time point), mice were anesthetized with isoflurane and the right and left TA muscles were injected with 50 µl of PBS (Sham) or CTX (10 µM, L8102, Latoxan Laboratory). ABT-263 administration was performed as described previously (Chang et al., 2016; Demaria et al., 2014). Briefly, mice ($n = 8$–9 per group) were injected with CTX or PBS (Sham control) as described above, and 3 days later, mice were gavaged daily with vehicle solution (Phosal, polyethylene glycol [PEG], and ethanol [EtOH] (60%:30%:10%)) or ABT-263 (Navitoclax, Toronto Research Chemicals A112500, 50 mg/kg) dissolved in vehicle for 7 or 15 days after which TA muscles were collected. Flash frozen, gastrocnemius muscles from male, 8-week-old D2.B10-Dmd^{mdx}/J (D2-*mdx*; $n = 4$) (Jackson Laboratories, stock # 013141), and DBA/2J (Jackson Laboratories stock # 000671) were generously provided by Dr. Vladimir Ljubicic (McMaster University).

2.2 | Mononuclear cell isolation

Muscle mononuclear cells were isolated as described previously[12,13] with slight modifications. Briefly, 5 days following CTX or Sham injection, TA muscles were isolated in a small biopsy dish where blood vessels, fat, and connective tissue were dissected away from the muscle. Samples were mulched in dissociation media (10 mg/ml Collagenase D [Roche], 4.8 U/ml Dispase II [Roche], and 10% horse serum in high-glucose DMEM) with fine scissors and incubated at 37°C for 45 min with agitation. Collagenase/dispase was inactivated with FBS, and the cells were filtered through a 40 µm strainer and centrifuged for 10 min at 1000 *g* at 4°C, washed in PBS, and underwent red blood cell lysis (Qiagen) and myofiber debris removal (Miltenyi Biotec, 130-109-398) using commercial kits following the manufacturer's instructions. Cell viability was >90% based on trypan blue staining in all samples. Cells were fixed in ice-cold methanol for 15 min on ice and stored at −80°C until scRNAseq analysis ($n = 5$ mice/preparations in each group [sham or CTX] and biological replicates were pooled immediately prior to methanol fixation).

2.3 | Single-cell and spatial RNA sequencing

Cells were recovered from methanol and processed as per the manufacturer's instructions (https://support.10xgenomics.com/single-cell-gene-expression/sample-prep/doc/demonstrated-protocol-methanol-fixation-of-cells-for-single-cell-rna-sequencing, 10X Genomics, Pleasanton, CA). Briefly, cells were removed from methanol through centrifugation and rehydrated in wash/suspension buffer (0.04% BSA, 1 mM DTT, 0.2 U/µl RNAse inhibitor in 3X SSC Buffer [in nuclease free water]) at a concentration of at least 500 cells/µl. scRNAseq, including droplet collection, cDNA amplification, and library preparation was carried out at the Princess Margaret Genomics facility (Toronto, ON) using the 10X Genomics Chromium system as per the manufacturer's guidelines (using PN-1000092). Resulting libraries were sequenced on an Illumina HiSeq2500 at the Princess Margaret Genomics facility (Toronto, ON) and FASTQ sequencing reads were processed, aligned to the mouse genome (mm10), and converted to digital gene expression matrices using the Cell Ranger count function within the Cell Ranger Single-Cell Software using the manufacturers' recommendations (https://support.10xgenomics.com/single-cell-gene-expression/software/overview/welcome).

For spatial transcriptomic analysis, the gastrocnemius of 8-week-old D2-*mdx* mice was isolated, embedded in OCT and flash-frozen in liquid nitrogen cooled, 2-metylbutane and cut at 10 µm into sections on 10x Visium gene expression slides, and processed for H&E staining. cDNA libraries with spatial tagging were built using the Visium Spatial Gene Expression 3' Library Construction v1 Kit (10x Genomics, Pleasanton, CA) and sequenced using a NovaSeq 6000 (Princess Margaret Genomics facility, Toronto, ON). Fiducial frames were manually aligned and spots in contact with the tissue section were selected using Loop Browser software (v4.0.0). Sequencing was aligned to the mouse genome (mm10) using spaceranger v1.0.0 which generated a feature-by-spot barcode expression matrix.

2.4 | Bioinformatic analysis

All downstream bioinformatic analysis was performed with R/RStudio (versions 3.6.3/1.3.1093) using Seurat version 3.1[14] which included quality control filtering, clustering, visualization, integration of data, and differential expression testing. Individual scRNAseq data sets underwent quality control filtering which removed genes expressed in less than 3 cells and cells that had unique molecular identifier (UMI) counts of <200 and >2500 as well as cells in which 20% of UMIs mapped to mitochondrial genes.[15,16] scRNAseq data sets were log normalized and variable features assessed prior to integration and batch correction using Seurat's "IntegrateData" function which is based on canonical correlation analysis and feature anchors. Data were scaled, and a principal component analysis (PCA) was performed on the expression matrix and the first 20 principal components were used for clustering at a resolution of 0.25 using Seurat's "FindNeighbors" and "FindClusters" functions. Visualization was carried out using uniform manifold approximation and projection (UMAP).[17] Unique cluster markers were determined by performing Seurat's "FindAllMarkers" function which only considers genes with $>\log_2(0.25)$ fold-change and expressed in at least 25% of cells in the cluster. To identify differentially expressed genes within a given cell type across conditions, Seurat's "FindMarkers" function was performed using the "RNA assay." To gain greater resolution in identifying immune cell types, uninjured and CTX data sets were analyzed separately and underwent clustering using the first 17 PCA dimensions (0.4 resolution) and 15 dimensions (0.3 resolution) respectively. Clusters identified as immune related were then subsetted and reclustered independently (control 15 dimensions, 0.2, CTX 10 dimensions, 0.3 resolution) prior to cluster identification as described above.

Spatial RNA sequencing analysis was performed using scanpy[18] version 1.8.2. Spots with less than 1000 UMIs or 500 unique genes were removed prior to preprocessing, embedding, and clustering. After per-spot counts per million normalization, data were log-transformed and PCA was performed with the 2000 most variable genes. Dimensionality reduction using UMAP was done using the top 50 principal components to build the neighbors graph, and clustering was done using the Leiden algorithm with 0.20 resolution for CTX-injected muscles and 0.30 for *mdx* muscle. For each data set, a list of spatially variable genes were found using SpatialDE2. Gene ontogeny (GO) terms were then generated by testing the spatially variable gene list against common (MSIGDB:H) and known senescence (MSIGDB:M9143, MSIGDB:M27187) gene sets using a hypergeometric test. Senescence and SASP scores were generated on a per-spot basis using scanpy's "score_genes" function, using senescence (MSIGDB:M9143) and SASP (MSIGDB:M27187) gene sets. Cluster-level senescence and SASP scores were then compared using the Wilcoxon rank-sum test using SciPy version 1.6 and Python version 3.7.0.

A panel of 29 senescence-related genes was used for analysis in Figure 4G by summing the average expression of all detected genes in Figure 4F, while significant

differences ($p < .05$) were examined between uninjured and CTX cells using the Wilcoxon rank-sum test using GraphPad Prism software (Version 6.01, GraphPad Software Inc., San Diego, CA).

2.5 | Immunohistochemistry

TA muscles were either fixed in 4% PFA for 24 h at 4°C or immediately flash frozen in liquid nitrogen cooled isopentane and stored at −80°C in optimal cutting temperature compound (OCT) prior to cryosectioning (7 μM sections). Since immunohistochemical (IHC) staining of tissue cross sections is not amenable following SA-β-gal detection, serial sections were generated, and SA-β-gal detection was performed on one section while the adjacent section underwent IHC staining after which colocalization was determined manually through image overlay. For IHC, detailed protocols are found in Table 1. Briefly, frozen sections were air-dried and fixed in 4% PFA or ice-cold acetone for 5 min at room temperature followed by 3, 5 min washes in 0.02% tween in PBS (PBS-T). Sections were permeabilized for 10 min with Triton-X 100 in PBS-T and incubated in the appropriate blocking solution for 1 h at room temperature. Slides were then incubated overnight with the primary antibody in blocking solution at 4°C. The next day, sections were washed three times for 5 min with PBS-T and incubated with the appropriate Alexa-conjugated secondary antibodies (Thermo Fisher) for 1–2 h in 2% BSA in PBS. Sections were again washed in PBS-T and counterstained with the nuclear marker DAPI and mounted. For the staining of SA-β-gal coupled with F480 in experiments utilizing ABT-263, serial sections were generated and SA-β-gal detection was performed on one section while the adjacent section underwent colorimetric IHC staining using the Vectastain Elite ABC kit (PK-6104) using the Vectastain DAB substrate kit for visualization (SK-4100) following the manufacturer's instructions.

2.6 | Single-molecule fluorescence in-situ hybridization

TA muscles from 8-week-old WT mice were injected with CTX, isolated 5 days later and flash-frozen as described earlier. Similarly, gastrocnemius muscles from 8-week-old control or D2-*mdx* mice were isolated and flash-frozen as described earlier. Seven micrometer sections were generated and were probed for *Cdkn1a* (Cat no. 408551) *Cdkn2a* (Cat no. 411011-C3), or *Trp53* (Cat no. 402331-C2) as per the manufacturer's instructions (ACD Bio, RNAscope Fluorescent Multiplex Assay Cat no. 320850) followed by IHC for PDGFRα or F4/80 as described in Table 1.

TABLE 1 Immunohistochemical procedures

Primary antibody (1°Ab)	1°Ab Source	Secondary antibody (2°Ab)	2°Ab Source	Fixation condition	Permeabilization and/or Block	1°Ab concentration	2°Ab concentration	3°Ab concentration
Rat anti-CD31	Abcam (ab56299)	Donkey anti-rat 488	Invitrogen (A21208)	Acetone	0.1% Triton 5% Donkey Serum	1:500	1:1000	--
Rat anti-F4/80	Bio-Rad (MCA497R)	Donkey anti-rat 488	Invitrogen (A21208)	2% PFA	5% Donkey Serum	1:250	1:1000	--
Rabbit anti-Laminin	Abcam (ab11575	Donkey anti-rabbit 488	Invitrogen (A21206)	4% PFA	0.1% Triton 5% Donkey Serum	1:1000	1:1000	--
Mouse anti-PDGFRα	R&D (AF1062)	2°Ab: Horse anti-goat biotin 3°Ab: Streptavidin 594	2°Ab: Vector Laboratories (BA-9500) 3°Ab: Invitrogen (S32356)	2% PFA	0.1% Triton DAKO serum-free block	1:500	1:250	1:1000
Mouse anti-Pax7	DHSB	2°Ab: M.O.M. Biotinylated antimouse 3°Ab: Streptavidin 594	2°Ab: Vector (MKB-2225) 3°Ab: Invitrogen (S32356)	2% PFA	0.2% Triton M.O.M. Block	1:2	1:250	1:250

2.7 | SA-β-gal assay

To quantity the number of SA-β-gal-positive cells following CTX or Sham injection, TA muscles were immersed in 4% PFA at 4°C for 24 h followed by cryoprotection in 30% sucrose for 24 h and freezing at described above. SA-β-gal detection was performed as previously described (Cazin et al. 2017; Le Roux et al. 2015). Sections were air-dried for 20 min, washed for 5 min with PBS, and then underwent 2, 5 min washes with PBS + MgCl2 (2 mM, pH 5.5). Sections were incubated in an X-gal solution containing 4 mM K3Fe(CN)6, 4 mM K4Fe(CN)6, 2 mM $MgCl_2$, and 400 μg/ml of x-gal powder in N-N dimethylformamide (16495-5, Cayman Chemical) in PBS, pH 5.5, at 37°C for a maximum of 24 h. Following incubation, slides were washed three times for 5 min each with PBS, with a final wash of PBS containing DAPI and then mounted using fluorescent aqueous mounting media (Thermo Fisher). For flash-frozen sections, SA-β-gal was detected in the same fashion with the exception of performing fixation with 1% PFA and 0.2% glutaraldehyde at the beginning and treatment with the X-gal substrate for 48 h (with a fresh substrate added at 24 h). Some sections were also counterstained with 0.5% eosin for 1 min, followed by a 2-min tap water rinse and dehydration in 95% and 100% ethanol and xylenes followed by mounting using nonaqueous mounting media. All sections were visualized using the Zeiss Axio Observer 7 (Axiocam, Carl Zeiss Microscopy, Jena, Germany) microscope with Zeiss ZEN software. ImageJ software (FIJI) was used for quantification of the images acquired.

2.8 | Muscle analysis

The average number of SA-β-gal positive cells were quantified across the regenerative time course and the experiments utilizing ABT-263 treatment in an area of 953361 μm^2. Time course experiments were analyzed with a one-way ANOVA followed by post-hoc analysis using the Tukey–Kramer multiple comparison test, while ABT-263 treatment experiments were examined using a two-tailed Student's *t* test. Morphometric analysis including quantification of Pax7-positive cells, Cd31-positive capillaries, and F4/80-positive macrophages was performed on an area encompassing a minimum of 150 fibers per mouse. Data analyses were conducted using GraphPad Prism software (Version 6.01, GraphPad Software Inc., San Diego, CA) with a p value of $\leq .05$ being deemed statistically significant while data are presented as the mean ± standard deviation of the mean.

2.9 | Cell proliferation assay

For in vitro cell proliferation, C2C12 myoblasts were seeded at a concentration of 1000 cells/well in a 96 well-plate and ABT263 (Cat no. A112500, Cedarlane Laboratories) was applied at increasing concentrations (0, 0.313, 0.625, 1.250, 2.5, and 5 μM) for 72 h. MTT assay (3 -(4,5-dimethylthiazol-2-yl)-2,5-diphenyltetrazolium bromide) was performed according to the manufacturer's instructions (Vybrant® MTT Cell Proliferation Assay Kit, Cat no. V-13154, Invitrogen). Briefly, media was replaced with 100 μl of fresh phenol red-free culture media (10% FBS Cat no. 12483-020, Thermo Fisher Scientific and 100 U/ml penicillin/streptomycin [P/S] Cat no. 15140-122, Thermo Fisher Scientific) and 10 μl of 12 mM of MTT stock solution was applied to each well. Following 2 h of incubation at 37 °C, cell culture media was removed and 50 μl of DMSO (Cat no. 85190, Thermo Fisher Scientific) was applied to each well followed by 10 min of incubation at 37°C. MTT absorbance was read at 540 nm on a POLARstar Omega plate reader (Cat no. S/N 415-0703, BMG LabTech). $N = 6$ each condition, with one-way ANOVA.

3 | RESULTS

3.1 | Spatial transcriptomics reveals senescence gene activity localized to areas of muscle repair

To investigate senescence throughout regenerative myogenesis, we assessed common senescence features across a time course of muscle repair, initially by examining the spatial expression of senescence genes in a published data set that utilized 10X based spatial transcriptomics following notexin injury (snake venom-derived myotoxin-based injury, similar to cardiotoxin) of mouse gastrocnemius muscles. As demonstrated by H&E staining, by 2 days post-injury there was focal muscle necrosis with distal areas of the muscle remaining intact (Figure 1B). By 5 days, inflammation in proximity to regions of newly formed myofibers was evident within areas damaged by notexin (Figure 1H). This is in agreement with spatial gene expression analysis which demonstrated that low-level clustering using Scanpy (1.8.2),[10] clusters corresponding to "uninjured" and "injured" regions were evident (Figure 1C,I, Figure S1A,B). For example, at 2 and 5 days, postinjury clusters demonstrated enhanced expression of inflammatory genes such as *Ctsb*, *Ly6e*, and *Apoe* and downregulation of muscle-related genes such as *Mb*, *Myh1*, and *Myh2* relative to uninjured clusters (Figure S1C,D). This was also evident by spatial feature plots that demonstrated localization of the macrophage marker *Cd68* to injured regions and *Myod1* and *Mhy3* to areas of regeneration (Figure S1E–L).

To examine how this relates to senescence, we first used an unbiased approach to identify genes that display spatial variability (i.e., genes that could potentially be

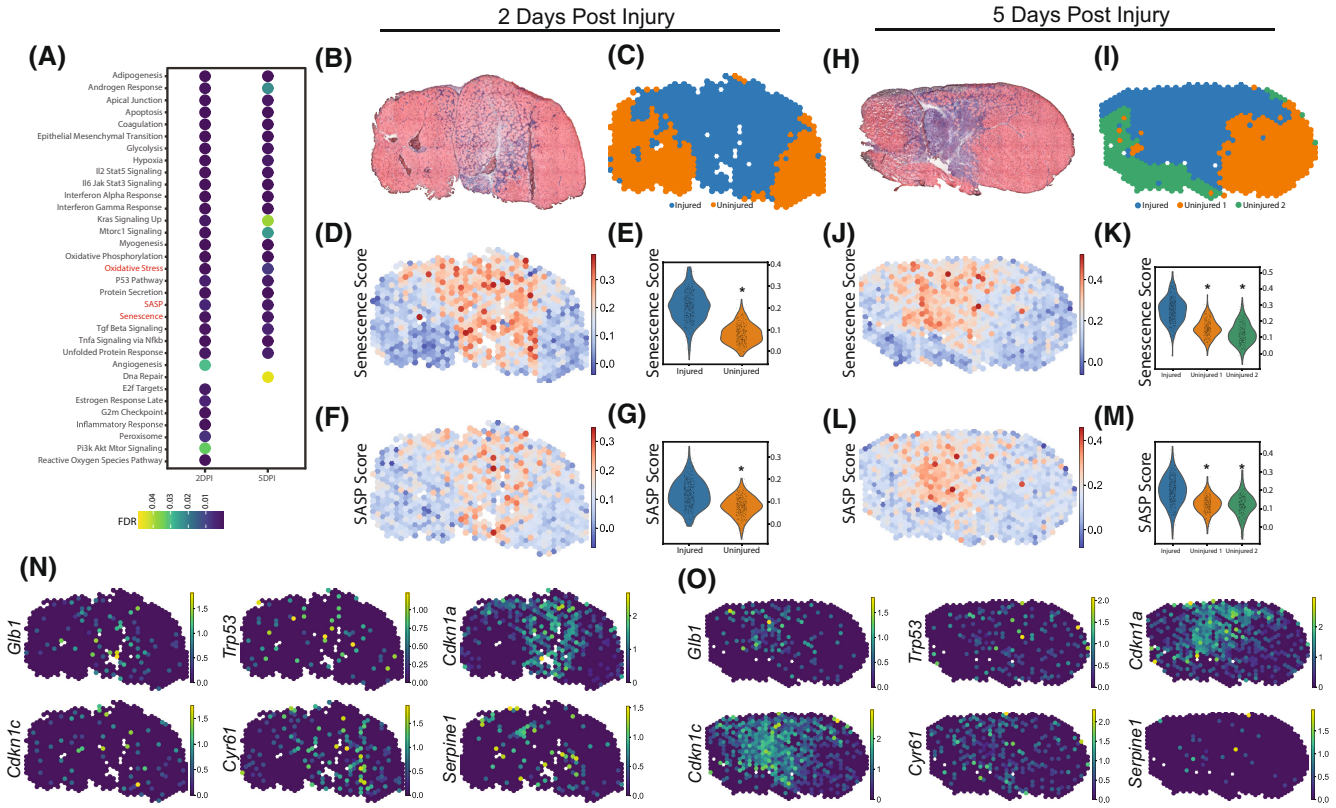

FIGURE 1 Spatial transcriptomics localizes senescence gene activity following muscle injury. (A) Gene Ontogeny analysis of spatially variable genes as identified by SpatialDE2 ($p < .05$, Benjamini-Hochberg correction (FDR <0.05) in the gastrocnemius muscle 2 and 5 days postnotexin injury based on spatial transcriptomics analysis. Hematoxylin and eosin images of gastrocnemius muscles (B and H) and spatial dimplots (C and I) localizing clusters at 2 and 5 days postnotexin injury, respectively. Senescence and SASP scores were calculated per gene expression spot and spatially localized to gastrocnemius muscles using spatial feature plots at 2 (D and F) and 5 (J and L) days postmuscle injury. Violin plots demonstrating the average Senescence and SASP scores per cluster at 2 (E and G) and 5 (K and M) days postmuscle injury. Spatial feature plots demonstrating the expression of the senescence-related genes, *Glb1*, *Trp53*, *Cdkn1a*, *Cdkn1c*, *Cyr61*, and *Serpine1* at 2 (N) and 5 (O) days postmuscle injury. *$p < .05$ compared with injured. Analysis of data published in[39] ($n = 1$ per time point).

restricted to damaged/undamaged areas of the muscle) by using SpatialDE2[19] at 2 and 5 days postinjury. Next, we generated GO terms based on significant spatially variable genes ($p < .05$) identified by SpatialDE2 which revealed expected terms such as "Inflammatory Response" "Myogenesis," "Mtorc1 signaling," and "Angiogenesis" (Figure 1A). Interestingly, there was also an overrepresentation of terms such as "SASP," "Senescence," "Oxidative Stress," "P53 Pathway," and "DNA repair." To better quantify and localize this, we created "Senescence" and "SASP" scores for each Visium gene expression spot based on the expression of genes associated with the GO terms Senescence and SASP using Scanpy's "score genes" function. This revealed concentrated expression of senescence and SASP genes to damaged and regenerating areas at 2 (Figure 1D,F) and 5 days postinjury (Figure 1J,L) and when calculated as a mean for each cluster, demonstrated a significant upregulation within the injured clusters (Figure 1E,G,K,M).

Next, we explored the expression of senescence-related genes identified by SpatialDE2, many of which were localized to damaged or regenerating areas. This included *Glb1* (the gene responsible for SA-βgal activity), the senescence pathway genes *Trp53*, *Cdkn1a*, *Cdkn1c*, and the SASP factors *Cyr61* (CCN1) and *Serpine1* (PAI-1) at 2 and 5 days postmuscle injury (Figure 1N,O, respectively). We examined the coexpression of *Trp53*, *Cdkn1a*, and *Glb1*, acknowledging the fact that Visium spots are large enough to contain the transcriptomes of more than one cell. This demonstrated that at 2 days postmuscle injury, of the spots that contained *Trp53* expression, 47% co-expressed *Cdkn1a*, 15% co-expressed *Glb1*, and 13% expressed all three genes. Similar results were observed 5 days postinjury. Of the spots that contained *Trp53* expression, 63% co-expressed *Cdkn1a*, 25% co-expressed *Glb1*, and 21% expressed all three genes. Taken together, these results demonstrate that a localized senescence response accompanies regenerative myogenesis.

3.2 | Myotrauma elicits dynamic cellular changes coincident with senescence activity

Visium spots are 55 μm in diameter and, therefore, represent gene expression of multiple cells. To identify which cells upregulate senescence-related genes, we performed high throughput, droplet-based scRNAseq to analyze transcriptomes of individual mononuclear cells prepared from Sham-injected (uninjured) and 5 days post-CTX-injected TA muscles (Figure 2A) as high senescence gene activity was observed at this time point (Figure 1). Using the R package Seurat 3.0,[12] we assessed 2578 cells from uninjured and 1013 cells from injured skeletal muscle with an average of 47 197 reads per cell with a median of 606 genes detected per cell. First, we classified the cellular response to muscle injury which revealed eight putative cell types across uninjured and injured muscles (Figure 2B,F–N, Figure S2A). This included *Pax7*-positive satellite cells (one cluster), *Pdgfra*-positive FAPs (two clusters), *Fmod*-positive tendon-like cells (one cluster), *Cdh5*-positive endothelial cells (one cluster), mural/smooth muscle mesenchymal cells expressing *Abcc9* (one cluster), muscle myonuclei expressing *Ckm and Des* (one cluster), *Plp1*-positive Schwann cells (one cluster), and immune cell populations (three

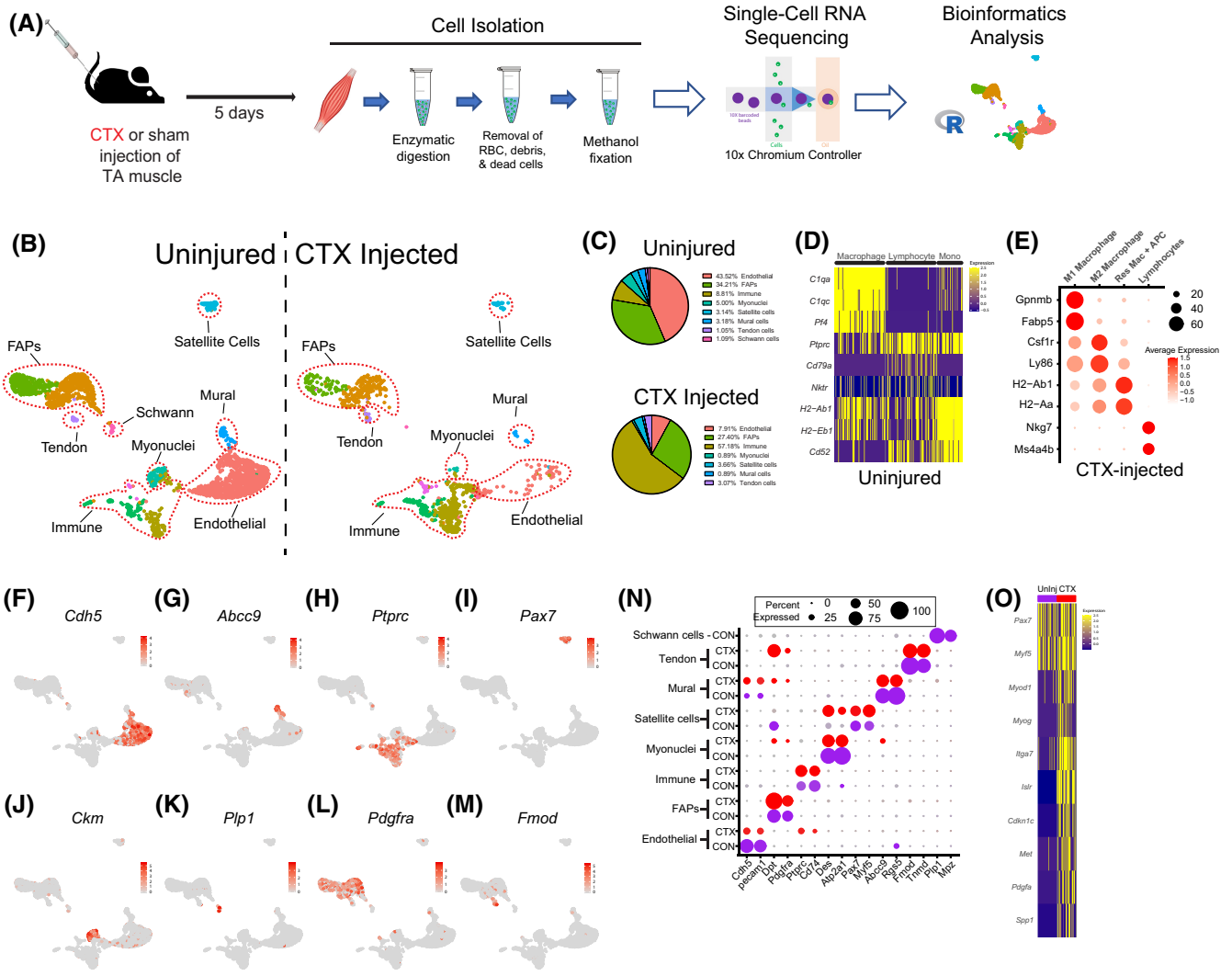

FIGURE 2 Skeletal muscle injury elicits dynamic cellular changes following cardiotoxin (CTX) injury. (A) Experimental workflow where mouse TA muscles were injected with PBS (sham) ($n = 5$ pooled) or CTX ($n = 5$ pooled) and collected 5 days later for enzymatic digestion, debris removal, and methanol fixation. Cells were recovered and subjected to scRNAseq and downstream bioinformatics analysis. (B) Uniform manifold approximation and projections to visualize cells from an integrated analysis of uninjured and CTX-injected muscles which identifies eight cell types and their proportions (C). Analysis of individual data sets reveals further resolution of immune cell types in uninjured (D) and injured (E) muscles. (F–M) Feature plots of cell type markers in combined data. (N) Dot plot of differentially expressed genes that distinguish cell populations in CON- (uninjured) and CTX-injected muscles. (O) Single-cell heatmap of myogenic genes in uninjured and CTX-injected muscles.

clusters), some of which expressed the pan-lymphocyte marker *Ptprc*.

In comparison with uninjured muscle, CTX injection elicited substantial and dynamic changes in many of these populations (Figure 2C) including endothelial cells, which were initially the most abundant (43% of cells) but were substantially decreased (8%) following injury, consistent with previous observations.[13] Conversely, immune cells accounted for the majority of cells following CTX injection (62%) but were sparse in uninjured muscle (~9% of total cells). Initially, immune cells grouped into three clusters (Figure S2B) which corresponded with resident macrophages (which clustered with platelets), lymphocytes, and a group of monocytes (Figure 2D). Following injury, four clusters of immune cells were present (Figure S2C), including M2 macrophages, pro-inflammatory M1 macrophages, resident macrophages, antigen-presenting cells (APCs), and a cluster of lymphocytes (Figure 2E). FAPs represented the next most abundant cell population in uninjured and injured muscle accounting for 34% and 27% of cells, respectively (Figure 2C). Satellite cells underwent dynamic transcriptional changes, as in uninjured muscle, most cells were quiescent and expressed *Pax7* and *Myf5*, while at 5 days post-CTX, they were proliferating and transitioning to differentiation with upregulations in *Myod1* and *Myog* (Figure 2O). This demonstrates that muscle injury elicits dynamic cellular changes in the muscle environment that coincides with heightened senescence gene activity.

3.3 | Multiple cell populations acquire senescent features following muscle injury

To investigate senescence, we analyzed the proportion of cells expressing canonical senescence pathway genes (Figure 3A).[6,20] In agreement with our spatial transcriptomics analysis, muscle injury increased the number of cells expressing *Cdkn1a* (2.8 fold), *Cdkn1b* (1.7-fold), *Cdkn1c* (1.2-fold), *Trp53* (2.2-fold), *Nfkb1* (2.2-fold), and *Glb1* (7.6 fold), while the number of cells expressing *Cdkn2a* ($p16^{INK4A}$) was low in both tissues. Gene expression overlayed on UMAPs (Figure 3B–E), using feature plots, demonstrated that each putative cell type demonstrated an increased proportion of cells expressing at least one senescence pathway gene, with most increasing the expression of multiple genes. In particular, immune cells, the vast majority of which were macrophages expressing *Adgre1* (F4/80) and *Ly86* and FAPs upregulated numerous senescence pathway genes such as *Cdkn1a* (immune), *Cdkn1b*, *Cdkn1c* (FAPs), *Trp53*, *Nfkb1*, and *Glb1* (FAPs and immune, respectively). While satellite cells upregulated *Cdkn1a*, *Cdkn1c*, and *Trp53*, these genes are known inducers of myoblast cell cycle withdrawal[21–23] and likely reflect cell differentiation/fusion. Indeed, smFISH of *Cdkn1a* revealed enriched expression in newly formed muscle fibers displaying central nucleation (Figure S3A). Additionally, *Glb1* was increased in each cell type following muscle injury. We also quantified the number of cells co-expressing the senescence marker genes *Cdkn1a*, *Trp53*, and/or *Glb1*. This demonstrated that 1.9% of cells expressed *Cdkn1a* and *Trp53*, 3.4% of cells expressed *Cdkn1a* and *Glb1*, 2.6% expressed *Trp53* and *Glb1*, and 0.5% of cells expressed all three genes.

Since the genetic response of senescence is often heterogeneous, recent investigations have sought to elucidate a common gene signature to many cell types following senescence induction.[24] Therefore, we examined a panel of 29 of these proposed genes and calculated a cumulative score based on their expression (Figure 3G) which demonstrated a significant increase ($p < .05$) in a muscle injury in FAPs, tendon cells, mural cells, and satellite cells with a trend for an increase ($p < .08$) in immune cells.

Last, we looked at the SASP, acknowledging the overlap between SASP factors and the inflammatory response to muscle injury. Here, we observed increased SASP factor gene expression in many cell types following injury, including tendon, mural, and endothelial cells in addition to FAPs and immune cells (Figure 3H). Interestingly, many SASP genes were commonly upregulated across multiple cell types including *Mif*, a pro-inflammatory cytokine that promotes macrophage mobilization (all cell types), the angiogenic *Hif1a* (FAPs, tendon, mural, SCs), and the senescence inducing *Igfbp4* (FAPs, endothelial tendon, mural, SCs) (Figure 3I–L). There were significant increases in the ECM remodeling factors *Mmp14* (all cell types, Figure 3L) and *Timp1* (FAPs, tendon, mural, Figure 3M), as well as *Cyr61* (FAPs, mural, satellite cells, Figure 3N) which has recently been linked with senescence-induced neonatal heart regeneration.[8] It is challenging to compare "senescent-like" cells to their nonsenescent-like counterparts for a given cell type, both statistically and because there is no universal marker that identifies all senescent cells. Nonetheless, we compared macrophages expressing/not expressing the senescence gene *Cdkn1a*. This revealed that *Cdkn1a*-expressing macrophages had enhanced expression of senescence-related genes such as the stress response genes *Gadd45b* and *Ier3*, the chemokine *Ccl9*, and the transcription *Klf4* which have been implicated in senescence[25] a pro-inflammatory macrophage phenotype[26] and p21-regulated senescence,[27] respectively. Taken together, these findings demonstrate that senescence-like characteristics are elicited in several cell types by muscle injury as evidenced by enhanced expression of core senescence genes and SASP factors.

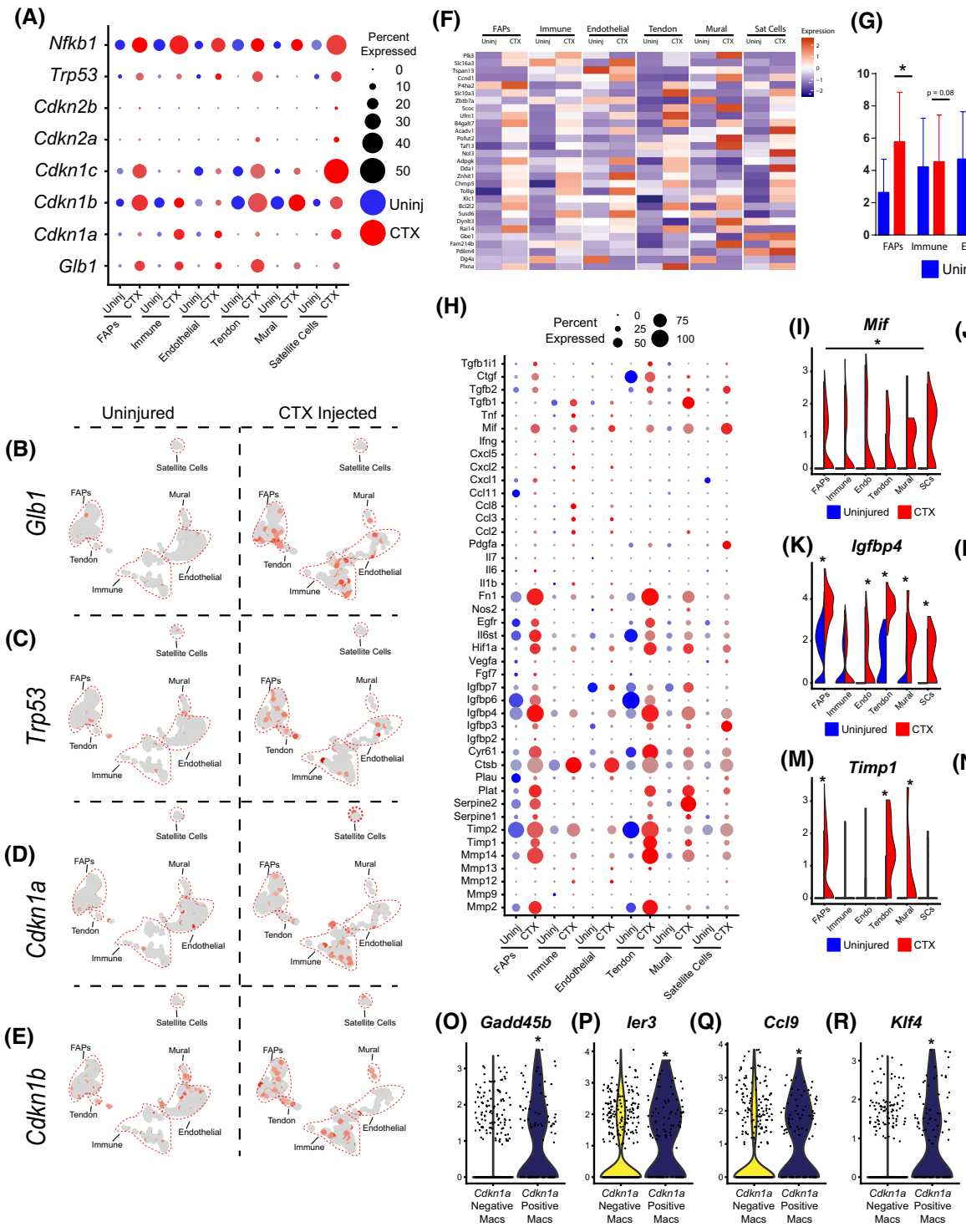

FIGURE 3 Muscle-derived senescent-like cells express characteristic senescence pathway genes and SASP factors. (A) Dot plot demonstrating the percentage of cells within each cluster expressing senescence genes across groups. Feature plots of *Glb1* (B), *Trp53* (C), *Cdkn1a* (D), and *Cdkn1b* (E) from uninjured (Sham-injected) and cardiotoxin (CTX)-injected muscle. (G) Cumulative gene expression based on 29 senescence-related genes (represented as a heatmap in F) in uninjured and CTX-injected samples. (H) Dot plot of SASP factor expression across cell types in uninjured and CTX-injected groups. Split-violin plots of the SASP factors *Mif* (I), *Hif1a* (J), *Igfbp4* (K), *Mmp14* (L), *Timp1* (M), and *Cyr61* (N) across cell types in uninjured and CTX-injected groups. Violin plots of *Gadd45b* (O), *Ier3* (P), *Ccl9* (Q), and *Klf4* (R) in *Cdkn1a*-positive and -negative macrophages 5 days post-CTX injection. Data in G are represented as the mean ± SD with $*p < .05$ compared with uninjured using the Wilcoxon rank-sum test ($n = 5$ mice per group). In I–N, $*p < .05$ of average gene expression compared to uninjured using the Wilcoxon rank-sum test with Bonferroni correction. In O–R, $*p < .05$ of average gene expression compared to *Cdkn1a*-negative cells using the Wilcoxon rank-sum test with Bonferroni correction.

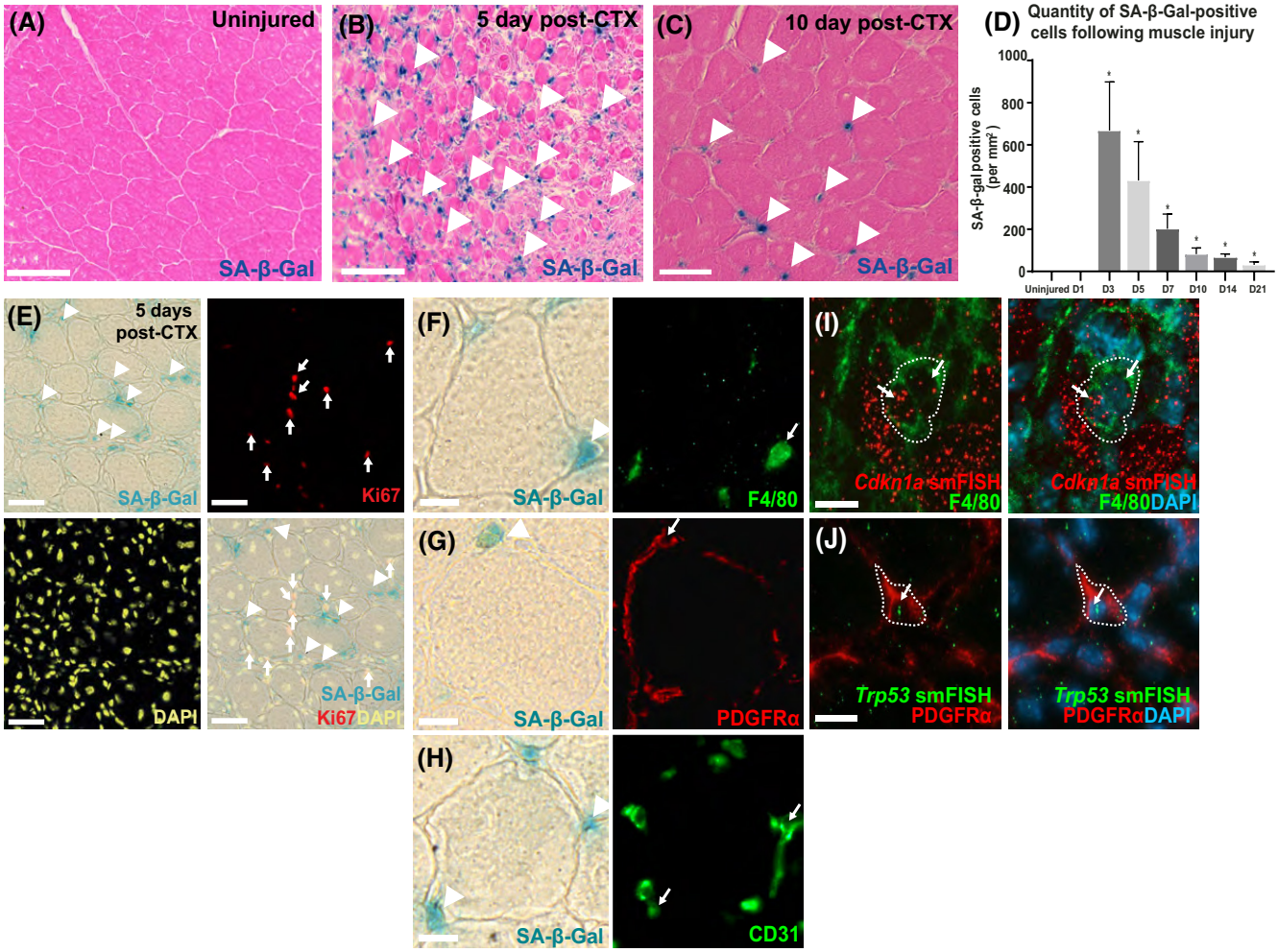

FIGURE 4 Cells with senescent features appear transiently in wild-type muscle following injury. Histological staining of SA-β-gal and eosin in Sham-injected (uninjured) (A) and cardiotoxin (CTX)-injected TA muscles isolated at days 5 (B) and 10 (C), postinjury. White arrowheads indicate SA-β-gal-positive cells. (D) Quantification of SA-β-gal-positive cells within TA muscles during regeneration ($n = 6–8$ mice per time point). SA-β-gal staining and IHC for Ki67 (E) in serial cross sections from 5 days post-CTX-injected muscle. White arrowheads indicate SA-β-gal-positive cells, whereas white arrows indicate Ki67-positive cells. Note, no colocalized cells were observed ($n = 3$ mice). Representative images of SA-β-gal staining of serial cross sections and IHC for F4/80 (F), PDGFRα (G), and CD31 (H). White arrowheads indicate SA-β-gal-positive cells, whereas white arrows indicate colocalization. Representative images of smFISH of *Cdkn1a* and IHC for F4/80 (I) and smFISH for *Trp53* and IHC for PDGFRα (J) demonstrate co-expression of senescence pathway genes in subsets of macrophages and FAPs 5 days post-CTX injection ($n = 4$ mice). Arrows indicate positive cells; hatched lines indicate areas of interest. A, B, C = 50 μm; E–J = 10 μm. Data in D and I are represented as the mean ± SD. *$p < .05$ compared with uninjured muscle.

3.4 | Cells with senescent features are transient following muscle injury

To better understand the kinetics of senescence-like cells following muscle injury we performed staining for the canonical senescence marker SA-β-gal[1,28,29] which was absent in noninjured muscle, as expected (Figure 4A). One day following CTX injury of mouse TA muscles, a timeframe typified by myofiber necrosis, almost no SA-β-gal-positive cells were present. However, at 3 days, there was an influx of Sa-β-gal-positive cells that peaked in abundance (667 ± 211 per mm^2), was maintained elevated at 5 days (430 cells per mm^2), and progressed back to near uninjured levels by 21 days (31 cells per mm^2) as muscle repair was completed (Figure 4B–D). Since senescent cells display halted cell cycle kinetics, we performed Ki67 immunostaining at 5 days postmuscle injury which demonstrated numerous positive cells (178.7 ± 11 cells per mm^2), however, none colocalized with SA-β-gal-positive cells (Figure 4E).

To help validate our scRNAseq results in vivo, we utilized two complementary approaches. First, since *Glb1* was increased in all cell types, we generated serial muscle cross sections from TA muscles injected with CTX 5 days prior and performed histology for SA-β-gal and IHC staining for cell type-specific markers. This revealed

colocalization of SA-β-gal-positive cells with the same major cell types identified by our scRNAseq analysis of *Glb1*-positive cells including F4/80-positive macrophages (9.4 ± 7.6% of F4/80-positive cells, Figure 4F), PDGFRα-positive FAPs (6.2 ± 2.4% of PDGFRα-positive cells, Figure 4G), CD31-positive endothelial cells (2.5 ± 0.64% of CD31-positive cells, Figure 4H) and no Pax7-positive satellite cells (Figure S3B). To find out whether the composition of the SA-β-gal-positive population changed throughout muscle regeneration, we performed a similar analysis 10 days post-CTX injection which revealed that endothelial cells (4.4 ± 1.4%), macrophages (16.5 ± 2.9%), and FAPs (3.1 ± 1.3%) were still the major populations while satellite cells or sublaminar myonuclei were not observed to colocalize with SA-β-gal. Since FAPs and immune cells encompassed the largest populations of cells with senescent-like features and had enhanced expression of *Trp53* and *Cdkn1a*, respectively, we performed IHC for PDGFRα and F4/80 in conjunction with smFISH (Figure 4I,J). This demonstrated that 23.6 ± 1.4% of macrophages expressed *Cdkn1a* and 30.2 ± 3.9% of FAPs expressed *Trp53* mRNA. Collectively, these data identify that injury to skeletal muscle induces the transient appearance of cells displaying senescent characteristics such as SA-β-gal activity, enhanced senescence gene activity, and blunted proliferation.

3.5 | Cells with senescent characteristics are heightened in dystrophic skeletal muscle

Next, we investigated if senescent-like responses across various cell types were exclusive to muscle regeneration following CTX-induced injury. To do this, we examined myopathic muscles from 8-week-old DBA (control) and D2-*mdx* mice, a rodent model of Duchenne Muscular Dystrophy which undergoes cyclic rounds of focal degeneration and repair.[30] First, we assessed SA-β-gal staining in D2-*mdx* mice which was absent in the control muscle (data not shown). In D2-*mdx* muscle, cells expressing SA-β-gal were abundant in areas of muscle fiber damage/repair (Figure 5A). Next, we performed spatial transcriptomics using 10x Visium to identify if regions undergoing muscle repair localize with senescence gene activity as they do in WT regenerating muscle. H&E staining (Figure 5B) and spatial feature plots clearly identify areas of focal damage/repair evidenced by enhanced gene activity localizing macrophage infiltration (*Cd68*, Figure 5C), myoblast activity and differentiation (*Myod1*, *Myog* Figure 5D,E respectively), and myofiber formation (*Myh3*) (Figure 5F). Further, following clustering based on spatial transcriptomics data (Figure S3C), spatial dim plots (Figure 5G) revealed two clusters aligning with inflammatory/regenerative regions which expressed *Apoe*, *Ctsb*, and *Cd68*, a cluster of uninjured muscle that was enriched for muscle genes such as *Ckm* and *Myh4* and a cluster where the majority of muscle fibers displayed central nucleation and expressed muscle related and myofiber maturation genes such as *Tnni2* and *Tnnc2* (Figure S3D).

As we did for WT regenerating muscle, we calculated senescence and SASP scores for each Visium spot which were used to calculate cluster averages. Visualizing these scores using feature plots demonstrated concentrated expression in regions undergoing active repair (Figure 5H,J) which is supported by the elevated scores in the clusters corresponding to the injured areas (Figure 5I,K). Using spatial feature plots, we visualized the expression of the key senescence genes such as *Cdkn1a*, *Trp53*, *Glb1*, and *Cdkn2d* and the SASP factors *CCN1* and *Serpine1* which were largely restricted to regions of inflammation and myofiber regeneration (Figure 5L–Q) while SpatialDE2 validated *Cdkn1a*, *Glb1, Cdkn2d, CCN1* and *Serpine1* as spatially variable genes. We also examined the co-expression of *Trp53*, *Cdkn1a*, and *Glb1*, which demonstrated that of the spots that contained *Trp53* expression, 50% co-expressed *Cdkn1a*, 15% co-expressed *Glb1*, and 10% expressed all three genes.

To learn the identity of cells expressing senescence-related genes, we performed smFISH for *Trp53* and *Cdkn1a* and focused on FAPs and macrophages based on our WT regeneration analysis. This revealed that within areas of active repair 21.4 ± 2.8% of F4/80-positive macrophages expressed *Cdkn1a* mRNA (Figure 5R), whereas a subset (18.9 ± 2.2%) of PDGFRα-positive FAPs expressed *Trp53* mRNA (Figure 5S). Altogether, these results demonstrate that SA-β-gal and senescence gene activity are present in dystrophic muscle with specific compartmentalization to regions of active muscle repair and inflammation.

3.6 | Senolytic treatment reduces SA-β-gal-positive cells and impairs muscle growth following injury

Based on previous reports, senescent-like cells could promote or inhibit tissue repair. To assess their functional role within the muscle, we treated mice with ABT-263 (Navitoclax), a senolytic compound that selectively eliminates senescent cells within numerous tissues, including skeletal muscle.[31,32] To test if ABT-263 ablates senescent-like cells during repair, we injected mouse TA muscles with CTX or PBS (sham control) and 3 days later administered vehicle or ABT-263 via gavage for 7 or 15 days as described previously[31,32] (Figure 6A). First, we tested if ABT-263 impacts uninjured skeletal muscle by examining muscle fiber CSA and Pax7-positive satellite cell content in the vehicle- and ABT-263-treated muscles. This demonstrated

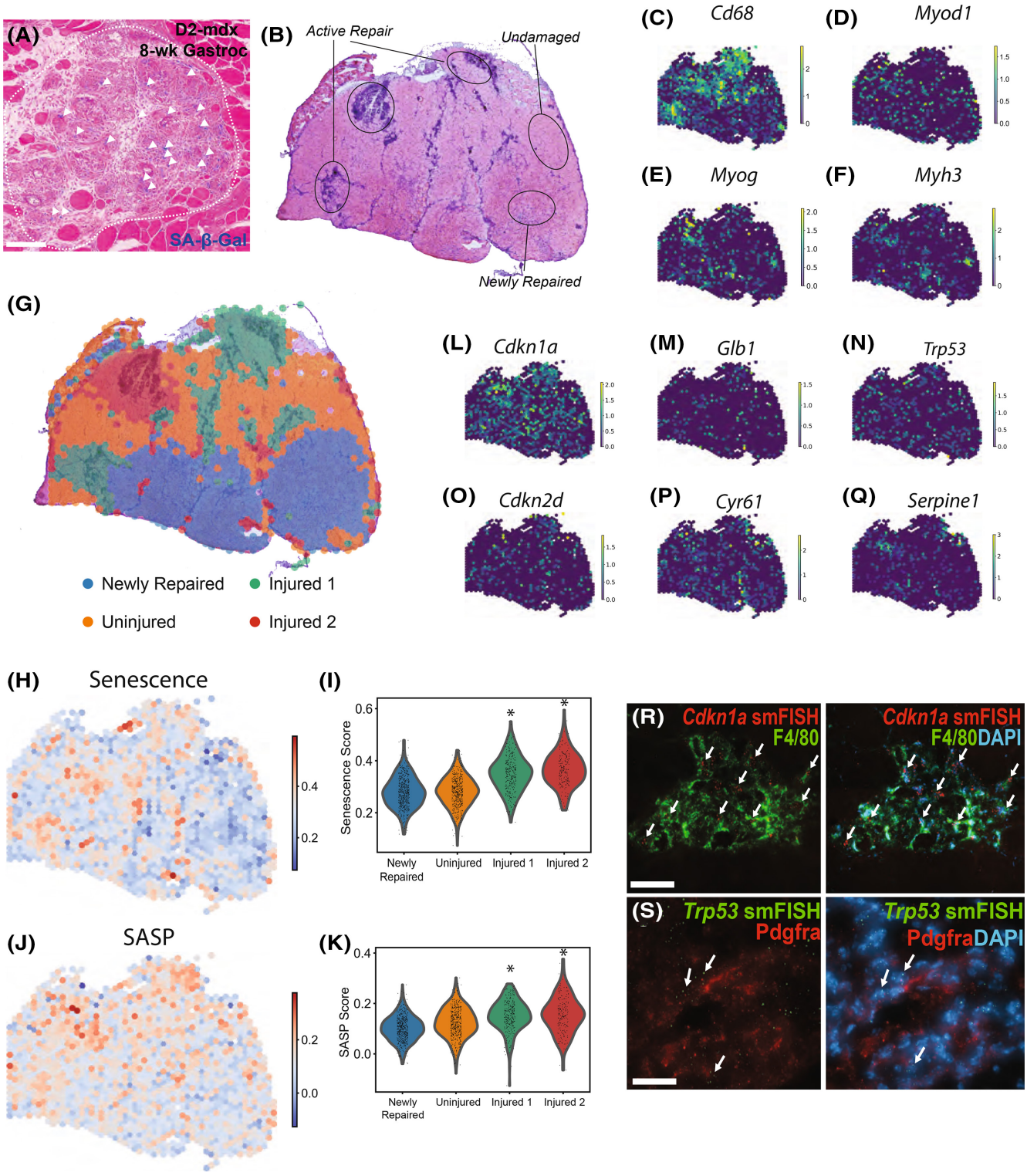

no differences across groups, suggesting that ABT-263 is not toxic at our treatment dose (Figure S4A,B). Next, we assessed injured skeletal muscles which showed that ABT-263 reduced the number of SA-β-gal-positive cells by 38% compared to vehicle-treated mice (Figure 6B–D, ABT-263 = 172.9 ± 63.4/mm^2; vehicle = 280.3 ± 66.4/mm^2, $p < .05$), suggesting it is partially effective at eliminating senescent-like cells.

We examined indices of muscle repair and growth in cross sections from vehicle- and ABT-263 treated mice at 10 days postinjury. We assessed muscle fiber CSA, which demonstrated a significant 25% reduction ($p < .05$, Figure 6E) in ABT-263-treated animals compared with vehicle-treated (vehicle = 887.12 ± 93.90 μm^2, ABT-263 = 667.96 ± 167.71 μm^2). In addition, the ABT-263-treated mice demonstrated a fiber CSA distribution that

FIGURE 5 Muscles of D2-*mdx* mice express senescence characteristics. (A) Representative image of histological staining of SA-β-gal and eosin in D2-*mdx* gastrocnemius muscles. Arrowheads demonstrate positive cells, whereas the hatched line highlights areas of repair/inflammation ($n = 4$ mice). (B) Hematoxylin and eosin image of 8-week-old D2-*mdx* gastrocnemius muscles utilized in spatial transcriptomics analysis. Circles indicate areas of active repair, newly repaired muscle fibers, or absence of muscle damage. (C–F) Spatial feature plots demonstrating gene expression of *Cd68*, *Myod1*, *Myog*, and *Myh3* in 8-week-old D2-*mdx* gastrocnemius muscles. (G) H&E image overlaid with a spatial dim plot localizing four clusters in 8-week-old D2-*mdx* gastrocnemius muscles. Senescence (H) and SASP (J) scores were calculated per gene expression spot and spatially localized to 8-week-old D2-*mdx* gastrocnemius muscles using spatial feature plots. Violin plots demonstrating the average Senescence (I) and SASP (K) scores per cluster in 8-week-old D2-*mdx* gastrocnemius muscles. Spatial feature plots demonstrating the expression of the senescence-related genes, *Cdkn1a*, *Glb1*, *Trp53*, *Cdkn1d*, *Cyr61*, and *Serpine1* in 8-week-old D2-*mdx* gastrocnemius muscles (L–Q, respectively). smFISH of *Cdkn1a* and IHC for F4/80 (R) and smFISH for *Trp53* and IHC for PDGFRα (S) demonstrating co-expression of senescence pathway genes in subsets of macrophages and FAPs in 8-week-old D2-*mdx* gastrocnemius muscles ($n = 3$ mice). Arrows indicate positive cells. Scale bars: A = 50 μm; R, S = 10 μm. *$p < .05$ compared with uninjured.

was skewed toward smaller fibers (Figure 6F). To better understand the relationship between senescent-like cell content and muscle fiber CSA, we performed Pearson's correlations with the vehicle- and ABT-263-treated animals which revealed a significant positive correlation between the number of SA-β-gal-positive cells and the average muscle fiber CSA (Figure 6G). ABT-263-treated mice also showed impaired myonuclear accretion as the average number of myonuclei per fiber was significantly reduced by 12% ($p < .05$) in comparison with vehicle-treated mice (Figure 6H) suggesting that satellite cell dynamics were impacted.

Therefore, we assessed the number of Pax7-positive satellite cells (Figure 6I,J) which was significantly ($p < .05$) reduced by 27% with ABT-263 treatment (Control – 12.6 ± 2.8 vs. ABT-263 – 9.9 ± 1.8 per 100 myofibers, Figure 6K). To assess if ABT-263 directly impacts myoblast proliferation, we treated C2C12 myoblasts with increasing doses of ABT-263 in culture based on previous studies.[31] This showed that cell proliferation was not impacted at physiological concentrations (0.31–1.25 μM) and only became impaired at the highest/toxic doses (2.5–5.0 μM) (Figure S4C). These results suggest that ABT-263 is not toxic to myoblasts. Next, we assessed if ABT-263 targets macrophages which were the most abundant SA-β-gal-positive population. This demonstrated that while total macrophage content was similar between vehicle- and ABT-263-treated mice (Figure S4D,E), the quantity of SA-β-gal-positive macrophages was significantly reduced (Figure 6L–N). ABT-263 treatment also had a nonsignificant effect on skeletal muscle capillarization (Figure S4F,G). We assessed muscle characteristics and satellite cell content again on day 18 postinjury. There was a 20% decrease in satellite cells per 100 fibers which trended to significance ($p = .1$) while muscle fiber CSA and nuclei per fiber were not significantly different across groups. (Figure S4H–J). This suggests that ABT-263 treatment could potentially have a longer-term impact on satellite cells but its overall effects on muscle fiber size are transient.

4 | DISCUSSION

Here we identify that following muscle injury, (1) a transient wave of cells demonstrating senescent characteristics such as senescence pathway expression, SA-β-gal activity, and SASP factor expression are present within skeletal muscle, (2) many cell types within skeletal muscle exhibit senescent characteristics with the largest populations being macrophages and FAPs, (3) this response is necessary for normal muscle repair and myonuclear accretion, and (4) cells within dystrophic muscle also exhibit senescence characteristics. Taken together, these results highlight an unexplored role for an "acute" senescence-like state in regulating muscle repair and expands the list of tissues such as skin[7] and neonatal heart[8] in which cellular senescence facilitates tissue regeneration. Our results also support a model where the downstream consequence of acquiring senescence characteristics may be context dependent and potentially dichotomous. Indeed, cells with senescence characteristics are present in both WT and dystrophic muscles. However, in WT muscle, these cells are largely transient, while they persist within the dystrophic muscle (at least until 8 weeks of age),[33] likely in response to constant degeneration and repair. What remains to be learned is if senescent-like cells in dystrophic muscle facilitate or impede the repair process. If the latter is true, treatment with senolytics like ABT-263 or dasatinib and quercetin[34] represents a novel, potentially translatable therapy.

The mechanisms which regulate the acute, injury-induced senescence-like state are currently unknown but may involve *Cdkn1a* ($p21^{Cip1}$), *Trp53* (p53), or potentially *Cdkn2a* ($p16^{INK4a}$). In aged skeletal muscle, satellite cells undergo "geroconversion" through upregulation of $p16^{INK4A}$ which ultimately limits self-renewal and a return to quiescence.[9] Here we show that many cell types acquire senescent features following acute muscle injury and upregulate *Cdkn1a* and/or *Trp53*, while *Cdkn2a* expression was not detected within our scRNAseq data and was rare in our spatial transcriptomics analysis, although increasing

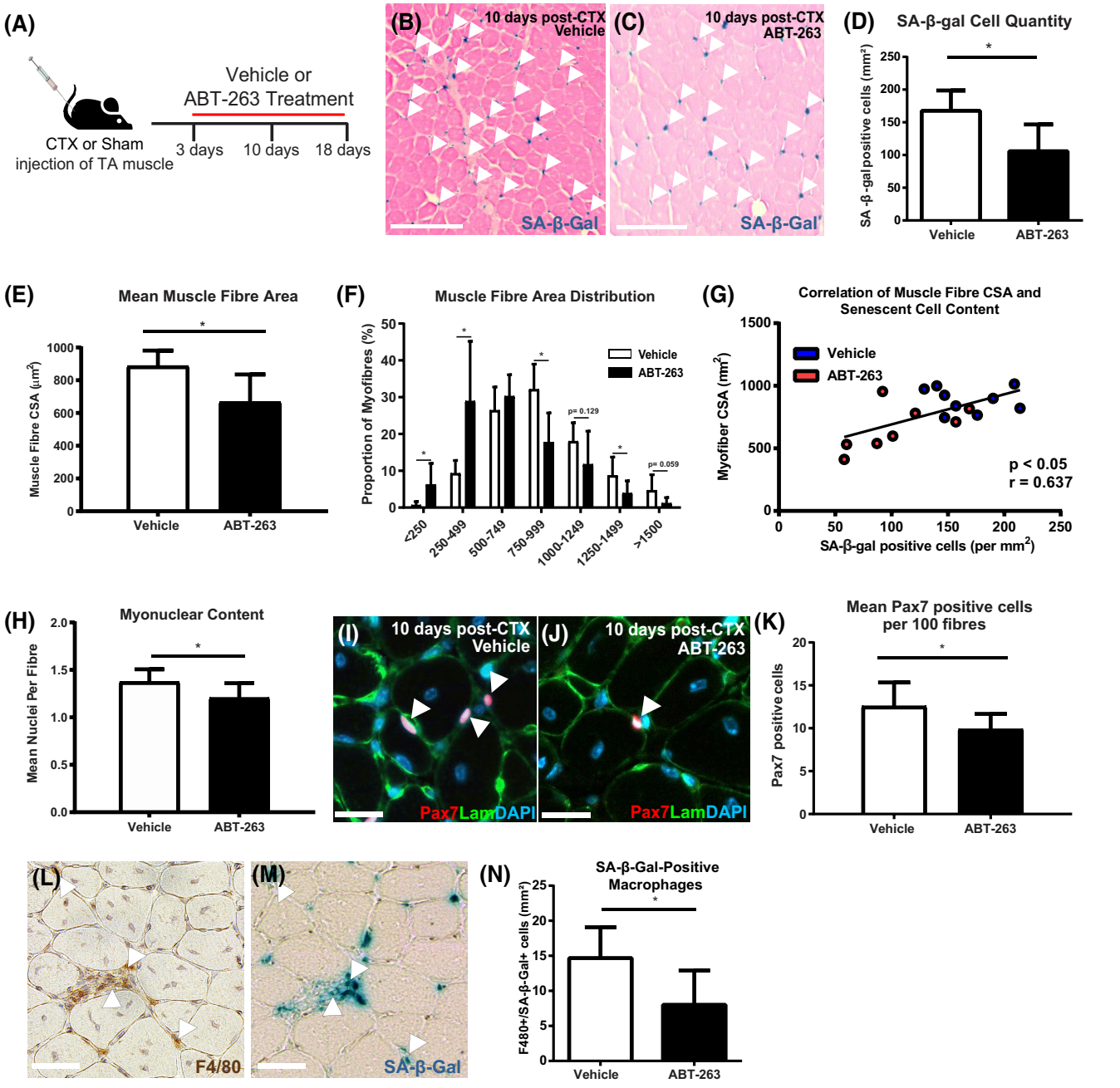

FIGURE 6 ABT-263 treatment decreases SA-β-gal-positive cells and impairs muscle growth following injury. Experimental time course where mouse TA muscles were injured with cardiotoxin (CTX) and 3 days later were treated with vehicle or ABT-263 for 7 or 15 days. Histological staining (B and C) and quantification (D) of SA-β-gal-positive cells in TA muscles at 10 days post-CTX-injury in vehicle- and ABT-263-treated mice. White arrowheads indicate SA-β-gal-positive cells. Quantification of mean muscle fiber cross-sectional area (E) and distribution (F) in vehicle- and ABT-263-treated mice 10 days post-CTX injection. (G) Pearson's correlation analysis demonstrated a positive correlation between muscle fiber CSA and the quantity of SA-β-gal-positive cells in vehicle- and ABT-263 treated mice 10 days post-CTX injection. Quantification of the mean number of myonuclei per muscle fiber (H). IHC staining (I and J) and quantification (K) of Pax7 to identify satellite cells in vehicle- and ABT-263-treated mice 10 days post-CTX injection (red = Pax7, green = laminin). IHC staining for F4/80 (L) and histological staining for SA-β-gal-positive cells (M) and quantification (N) in vehicle- and ABT-263-treated mice 10 days post-CTX injection (brown = F4/80, blue = SA-β-gal). Scale bars in I, J, L, M = 10 μm. All data correspond to the mean ± SD using $n = 8–9$ mice per group. *$p < .05$ compared with vehicle-treated mice.

following injury. *Cdkn2a* expression was also detected using smFISH and through spatial transcriptomics in D2-*mdx* muscle and appeared restricted to newly formed myofibers and some interstitial cells (identity currently unknown).

We hypothesize that senescent-like cells influence muscle repair through the secretion of SASP factors that likely serve multiple roles such as regulating the inflammatory response, facilitating ECM remodeling, and

providing trophic support for satellite cells. Indeed, we see the increased expression of inflammatory factors, cytokines, chemokines, MMPs, and TIMPSs in senescent-like cells following injury. Of note is the expression of *Cyr61* within regenerating WT and D2-*mdx* muscle which has been demonstrated as a necessary SASP factor, facilitating neonatal heart and skin regeneration.[8,35] However, further investigations using gain or loss of function experiments in specific senescent-like cell populations will be required to define the individual contributions of each cell type to muscle repair. Of particular interest are macrophages, which displayed SA-β-gal activity and the expression of SASP factors and *Cdkn1a*. However, recent work has identified that macrophages can reversibly upregulate the expression of another senescence gene, 16^{INK4A}, and gain SA-β-gal activity,[36] which not only underscores our need to develop new markers of senescence but highlights the "cellular flexibility" of macrophages. Therefore, whether the senescence-like state observed in macrophages following muscle damage is true senescence is debatable and may reflect just one of numerous macrophage activation states.[37] Further, recent work has also highlighted the role of exercise in promoting a senescence state in FAPs that benefits idiopathic inflammatory myopathy.[38] In conclusion, we provide evidence that acquired, acute senescence-like characteristics in multiple cell types function to regulate skeletal muscle growth and satellite cell abundance following injury. These findings, in concert with previous work, support a model that tissues with high regenerative capacity may rely on an acute senescence-like response to support tissue repair.

AUTHOR CONTRIBUTIONS

Laura V. Young performed the majority of the analysis, wrote, and edited the manuscript. Griffen Wakelin performed spatial transcriptomic analysis and edited the manuscript. Alasdair W. R. Cameron, Grant Wolters and Michel G. Arsenault, performed data analysis and edited the manuscript. Sean Ng isolated and prepared tissues from mice and edited the manuscript. Nicolás Collao performed cell culture proliferation assays and edited the manuscript. Vladimir Ljubicic provided tissues, consulted on analysis, and edited the manuscript. Joel P. Ross, J. Patrick Murphy, Stevan A. Springer, and Michael De Lisio consulted on analysis and edited the manuscript. Adam P. W. Johnston conceived the experiments, aided in analysis assisted in writing, and edited the manuscript.

FUNDING INFORMATION

This work was funded by an NSERC Discovery Grant (RGPIN-2016-05747). GW was funded through an NSERC Undergraduate Student Research Assistantship. NC is supported by the Chilean National Agency for Research and Development (ANID).

DISCLOSURES

The authors declare that they have no conflict of interest.

DATA AVAILABILITY STATEMENT

Spatial transcriptomics data of notexin-injured WT muscle is from[39] while spatial transcriptomics of D2-*mdx* and scRNAseq data will be uploaded to the GEO database prior to publication.

ORCID

Adam P. W. Johnston https://orcid.org/0000-0001-8875-6088

REFERENCES

1. Rodier F, Campisi J. Four faces of cellular senescence. *J Cell Biol*. 2011;192:547-556.
2. Zhang P, Kishimoto Y, Grammatikakis I, et al. Senolytic therapy alleviates Aβ-associated oligodendrocyte progenitor cell senescence and cognitive deficits in an Alzheimer's disease model. *Nat Neurosci*. 2019;22:719-728.
3. Shimizu I, Minamino T. Cellular senescence in cardiac diseases. *J Cardiol*. 2019;74:313-319.
4. Lee S, Schmitt CA. The dynamic nature of senescence in cancer. *Nat Cell Biol*. 2019;21:94-101.
5. Itahana K, Campisi J, Dimri GP. Mechanisms of cellular senescence in human and mouse cells. *Biogerontology*. 2004;5:1-10.
6. Herranz N, Gil J. Mechanisms and functions of cellular senescence. *J Clin Invest*. 2018;128:1238-1246.
7. Demaria M, Ohtani N, Youssef SA, et al. An essential role for senescent cells in optimal wound healing through secretion of PDGF-AA. *Dev Cell*. 2014;31:722-733.
8. Feng T, Meng J, Kou S, et al. CCN1-induced cellular senescence promotes heart regeneration. *Circulation*. 2019;139:2495-2498.
9. Sousa-Victor P, Gutarra S, García-Prat L, et al. Geriatric muscle stem cells switch reversible quiescence into senescence. *Nature*. 2014;506:316-321.
10. Noel T, Wang QS, Greka A, Marshall JL. Principles of spatial transcriptomics analysis: a practical walk-through in kidney tissue. *Front Physiol*. 2022;12:809346.
11. Moses L, Pachter L. Museum of spatial transcriptomics. *Nat Methods*. 2022;19:534-546.
12. Hindi L, McMillan JD, Afroze D, Hindi SM, Kumar A. Isolation, culturing, and differentiation of primary myoblasts from skeletal muscle of adult mice. *Bio Protoc*. 2017;7:e2248.
13. Motohashi N, Asakura Y, Asakura A. Isolation, culture, and transplantation of muscle satellite cells. *J Vis Exp*. 2014;(86):50846.
14. Butler A, Hoffman P, Smibert P, Papalexi E, Satija R. Integrating single-cell transcriptomic data across different conditions, technologies, and species. *Nat Biotechnol*. 2018;36:411-420.
15. De Micheli AJ, Laurilliard EJ, Heinke CL, et al. Single-cell analysis of the muscle stem cell hierarchy identifies heterotypic communication signals involved in skeletal muscle regeneration. *Cell Rep*. 2020;30:3583-3595.e5.
16. Giordani L, He GJ, Negroni E, et al. High-dimensional single-cell cartography reveals novel skeletal muscle-resident cell populations. *Mol Cell*. 2019;74:609-621.e6.

17. Becht E, McInnes L, Healy J, et al. Dimensionality reduction for visualizing single-cell data using UMAP. *Nat Biotechnol*. 2019;37:38-44.
18. Wolf FA, Angerer P, Theis FJ. SCANPY: large-scale single-cell gene expression data analysis. *Genome Biol*. 2018;19:15.
19. Kats I, Vento-Tormo R, Stegle O. SpatialDE2: Fast and localized variance component analysis of spatial transcriptomics. *bioRxiv*. 2021;2021.10.27.466045.
20. Campisi J, d'Adda di Fagagna F. Cellular senescence: when bad things happen to good cells. *Nat Rev Mol Cell Biol*. 2007;8:729-740.
21. Flamini V, Ghadiali RS, Antczak P, Rothwell A, Turnbull JE, Pisconti A. The satellite cell niche regulates the balance between myoblast differentiation and self-renewal via p53. *Stem Cell Rep*. 2018;10:970-983.
22. Mademtzoglou D, Asakura Y, Borok MJ, et al. Cellular localization of the cell cycle inhibitor Cdkn1c controls growth arrest of adult skeletal muscle stem cells. *Elife*. 2018;7:e33337.
23. Porrello A, Cerone MA, Coen S, et al. P53 regulates myogenesis by triggering the differentiation activity of Prb. *J Cell Biol*. 2000;151:1295-1304.
24. Hernandez-Segura A, de Jong TV, Melov S, Guryev V, Campisi J, Demaria M. Unmasking transcriptional heterogeneity in senescent cells. *Curr Biol*. 2017;27:2652-2660.e4.
25. Magimaidas A, Madireddi P, Maifrede S, Mukherjee K, Hoffman B, Liebermann DA. Gadd45b deficiency promotes premature senescence and skin aging. *Oncotarget*. 2016;7:26935-26948.
26. Orecchioni M, Ghosheh Y, Pramod AB, Ley K. Macrophage polarization: different gene signatures in M1(LPS+) vs. classically and M2(LPS-) vs. alternatively activated macrophages. *Front Immunol*. 2019;10:1084.
27. Xu Q, Liu M, Zhang J, et al. Overexpression of KLF4 promotes cell senescence through microRNA-203-survivin-p21 pathway. *Oncotarget*. 2016;7:60290-60302.
28. Biran A, Zada L, Abou Karam P, et al. Quantitative identification of senescent cells in aging and disease. *Aging Cell*. 2017;16:661-671.
29. Noren Hooten N, Evans MK. Techniques to induce and quantify cellular senescence. *J Vis Exp*. 2017;(123):55533.
30. Fukada S, Morikawa D, Yamamoto Y, et al. Genetic background affects properties of satellite cells and mdx phenotypes. *Am J Pathol*. 2010;176:2414-2424.
31. Chang J, Wang Y, Shao L, et al. Clearance of senescent cells by ABT263 rejuvenates aged hematopoietic stem cells in mice. *Nat Med*. 2016;22:78-83.
32. Chiche A, Le Roux I, von Joest M, et al. Injury-induced senescence enables in vivo reprogramming in skeletal muscle. *Cell Stem Cell*. 2017;20:407-414.e4.
33. Young LV, Morrison W, Campbell C, et al. Loss of dystrophin expression in skeletal muscle is associated with senescence of macrophages and endothelial cells. *Am J Physiol Cell Physiol*. 2021;321:C94-C103.
34. Hickson LJ, Langhi Prata LGP, Bobart SA, et al. Senolytics decrease senescent cells in humans: preliminary report from a clinical trial of Dasatinib plus quercetin in individuals with diabetic kidney disease. *EBioMedicine*. 2019;47:446-456.
35. Jun J-I, Lau LF. The matricellular protein CCN1/CYR61 induces fibroblast senescence and restricts fibrosis in cutaneous wound healing. *Nat Cell Biol*. 2010;12:676-685.
36. Hall BM, Balan V, Gleiberman AS, et al. p16(Ink4a) and senescence-associated β-galactosidase can be induced in macrophages as part of a reversible response to physiological stimuli. *Aging*. 2017;9:1867-1884.
37. Behmoaras J, Gil J. Similarities and interplay between senescent cells and macrophages. *J Cell Biol*. 2020;220:e202010162.
38. Saito Y, Chikenji TS, Matsumura T, Nakano M, Fujimiya M. Exercise enhances skeletal muscle regeneration by promoting senescence in fibro-adipogenic progenitors. *Nat Commun*. 2020;11:889.
39. McKellar DW, Walter LD, Song LT, et al. Strength in numbers: large-scale integration of single-cell transcriptomic data reveals rare, transient muscle progenitor cell states in muscle regeneration. *bioRxiv*. 2020:34773081.

SUPPORTING INFORMATION

Additional supporting information can be found online in the Supporting Information section at the end of this article.

How to cite this article: Young LV, Wakelin G, Cameron AWR, et al. Muscle injury induces a transient senescence-like state that is required for myofiber growth during muscle regeneration. *The FASEB Journal*. 2022;36:e22587. doi: 10.1096/fj.202200289RR